Study of a Lifted-Jet Flame using a Stereoscopic PIV System

by

Donghee Han[1], L. K. Su[2], R. K. Menon[3] and M. G. Mungal[1]

[1] Mechanical Engineering Department, Stanford University,
Stanford, CA 94305, USA

[2] Center for Turbulence Research, Stanford University,
Stanford, CA 94305, USA

[3] TSI Incorporated, St. Paul, MN 55126, USA

ABSTRACT

Three components of the velocity field at the base of a lifted flame have been measured using stereoscopic particle image velocimetry (SPIV). The validity of applying the SPIV technique in the presence of a flame has been assessed. It has been found that the change of the index of refraction due to the presence of the flame, when compared to a non-reacting flow, can distort the PIV image as much as 1 pixel. However, the distortion between consecutive PIV images could be greatly minimized if the time delay between the two images is within the order of milliseconds. In this work, the instantaneous and the ensemble averaged three-component velocity and the turbulent quantities at the flame base of a lifted flame have been measured. Complex three-dimensional structures are observed at the flame base including the meandering in both in and out of plane directions. Conditional axial velocity measurements at the flame base show similar results (mean speed of $2.4S_L$, where S_L is the laminar flame speed) with previous measurements. However, highest velocities in the radial and azimuthal directions are on the order of $2\sim3S_L$, which implies a possible role of these velocity components in flame stabilization. The turbulent kinetic energy distribution shows a sudden reduction when the flow encounters the flame base, which is thought to be due to the stabilizing effect of heat release.

1. INTRODUCTION

There have been many previous studies concerning the stabilization and blowout mechanism of turbulent lifted jet diffusion flames. Experimental and theoretical findings on the liftoff and blowout phenomena have been reviewed by Pitts (1988). The initial attempt to explain flame liftoff as the balance between the flow velocity and the turbulent flame speed at the flame base (Vanquickenborne and Van Tiggelen, 1966) has been questioned by various researchers. Other mechanisms considered as a possible stabilization mechanism include flamelet extinction by excessive strain rate (Peters and Williams, 1983), large scale turbulent structures (Broadwell et al., 1984), and more recently, the triple-flame-like turbulent leading edge flames (Müller et al., 1994; Muñiz and Mungal, 1997; Schefer and Goix, 1998; Maurey et al., 1998).

Among these, the stabilization mechanism by the turbulent leading edge flame relies upon modern experimental measurement techniques such as particle image velocimetry (PIV) and planar laser induced fluorescence (PLIF), which can locate the instantaneous position of the flame base and the two components of velocity at that location. However, it is known that the flame base of a lifted flame has a highly complex three-dimensional structure owing to the interaction of the turbulent flow with heat release, density change, and possible buoyancy, which results in limitations on understanding the liftoff and blowout phenomena. Even though the previous studies provided significant insight for understanding the liftoff problem, the three-dimensional structure and its role on the stabilization of a lifted flame have not been investigated in detail to our knowledge.

As a first step to understanding the complex three-dimensional structure of the lifted flame base, the stereoscopic particle image velocimetry (SPIV) technique is applied to measure the three components of the velocity field at different planes of the flame base of a lifted flame. In addition, the change of the refractive index, which occurs due to the heat release of a flame, impacts the implementation of the SPIV technique and has been investigated. Instantaneous and ensemble averaged three component velocity fields are presented and the turbulent kinetic energy distribution are obtained. The conditional velocity statistics at the instantaneous locations of the flame base are also reported.

2. EXPERIMENTAL METHOD

2.1 Experimental Facility

The experiment is performed in a vertical wind tunnel with a test section size of 30cm × 30cm and a 4

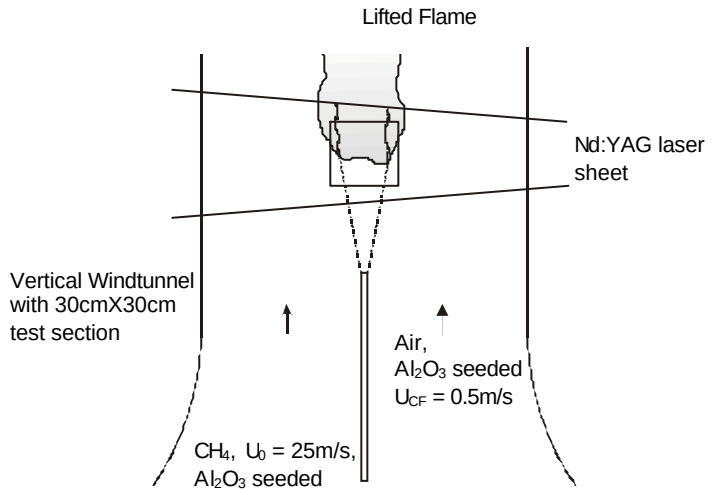

Fig. 1 Experimental facility.

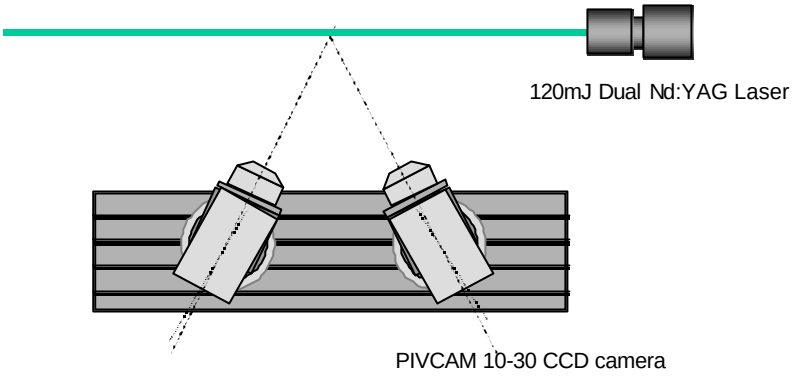

Fig. 2 Two-Camera Scheimpflug arrangement for stereoscopic PIV measurements.

to 1 contraction inlet, which is shown in Fig. 1. The fuel jet (99.5% CH_4) issues from a long tube (4.6mm inner diameter stainless steel) and the coflow speed can be adjusted. The nozzle exit velocity and its corresponding Reynolds number are 25m/s and 7000 respectively. The coflow speed is set to 0.5m/s and the corresponding average liftoff height was 110mm (x/d = 24).

Three-component velocity measurements are carried out using a SPIV system from TSI. Two progressive scan interline CCD cameras (PIVCAM 10-30, 1k×1k pixel resolution) are set up in the Scheimpflug configuration, which is known to be the optimal arrangement for SPIV measurements (Bjorkquist, 1998). The effect of the perspective viewing and the distortion associated with the camera configuration is handled by generating a mapping function following the calibration procedure by Soloff et al. (1997).

A 120mJ dual Nd:YAG laser system is used to illuminate the alumina (Al_2O_3) particles with nominal diameter of 5*m*m. A master control unit (TSI Model 610034 Synchronizer system) adjusts the time delay between the cameras and the laser. Particle images are processed by the standard cross-correlation algorithm in the TSI INSIGHT software package using a 32×32 pixel interrogation window size. Four processors are used in parallel by dividing an image into four different regions, which accelerates the image processing. The experimental setup used for the camera and the laser are shown schematically in Fig. 2. The tilt angles of the two cameras were 17° (left) and 15° (right) to the z axis. The three-component velocity measurements are made in streamwise planes at z = 0, 10, 20, and 27mm from the center plane of the jet.

2.2 Mapping function generation

Perspective imaging by the cameras in the Scheimpflug configuration associated with the stereoscopic PIV set up creates variable magnification. This results in the need to establish a unique relationship between the image and the object planes.

The mapping function provides a one-to-one relation between positions in the object plane to positions (pixels) in the image plane, taking into account all the factors including the effect of windows. This mapping of the object plane (plane of the light sheet) into the image plane is achieved in a systematic fashion.

A plate with a rectangular grid pattern is first aligned with the center plane of the light sheet and both cameras, used in the Stereoscopic arrangement, capture images of this plate. The grid pattern with the precisely defined nodal points becomes the calibration grid. To cover the thickness of the light sheet, the calibration plate is traversed and images captured using both cameras. An alternate approach is to use a calibration plate with grid points located at different depths (or thickness) to cover the thickness of the light sheet and then capture images using both cameras. The set of grid point locations and the corresponding images were used to generate calibration polynomial equations for each camera. In other words, these equations provide a one-to-one mapping of the points in the object plane to locations in the image plane.

The mapping function equations are used to go from the vectors obtained in the image plane locations to the corresponding points in the flow. The details of the mapping function generation and other details are provided by Soloff et al. (1998) and Bjorkquist (1997).

3. EFFECT OF THE REFRACTIVE INDEX CHANGE

Muñiz et al. (1996) have explored the effect of the refractive index change on the recording of particle images in a flame for PIV measurements. They have concluded that the image distortion effect can be insignificant when the index change occurs near the object plane (i.e. the laser-illuminated PIV particles themselves). Similar studies have been carried out here for the case of a SPIV system. For the case of SPIV measurements, two cameras capture the particles by viewing through different parts of the flame. Hence, the effect of the spatial variation of the refractive index on the images recorded by the cameras needs to be quantified.

In order to quantify the effect of the flame, images of a steel ruler have been recorded with and without a hydrogen flame. The steel ruler images with and without flame are divided into small regions (64 × 64 pixel correlation window) and a simple cross-correlation is performed in each region. This procedure provided the displacement caused by the index change. Figures 3(a) and 3(b) show the images of the steel ruler without and with the flame respectively. The result of the cross-correlation on these images is shown in Fig. 3(c). The displacements ranged from 0.2 to 0.9 pixels depending on the position, which can be a significant error for measuring small displacements. However, the same test performed between two images of the steel ruler with the H_2 flame, which are taken with 67ms of time delay, shows that the distortion due to the refractive index difference are relatively small (See Fig. 4).

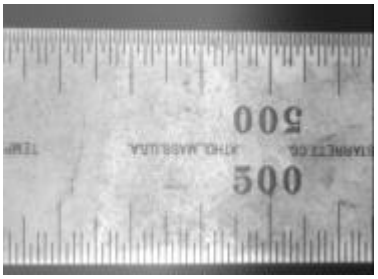

(a) Without H_2 Flame

(b) With H_2 Flame

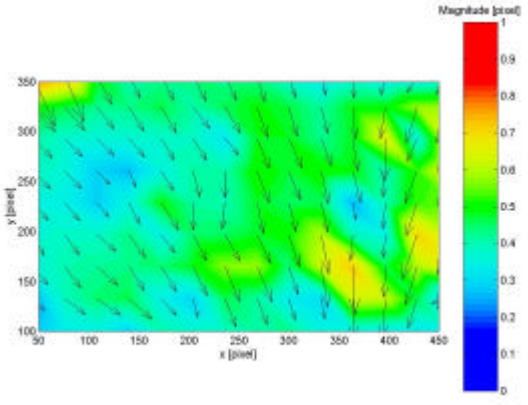

(c) Cross correlation of images (a) and (b)

Fig. 3 Distortion of the image due to heat release.

(a) With H_2 Flame at t

(b) With H_2 Flame at t+67ms

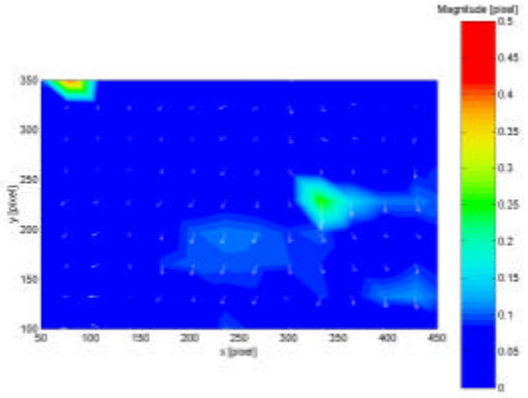

(c) Cross correlation of images (a) and (b)

Fig. 4 Distortion of the image between short time interval with the flame.

In most locations of the image, the displacements are within 0.1 pixels. Considering the time delay between two images in the actual experiment is significantly smaller (Dt = 60ms), the error in measuring the displacement will not be significant even under flame conditions. If we assume that the displacement of particles can be measured acceptably, the remaining source of error will be from the registration of the images from the two cameras. Since the maximum distortion by the flame was around 1 pixel in Fig. 3, the registration error will be of the same order. Since the mapping function uses a third order polynomial, which is a smooth function, 1 pixel displacement will not cause a significant difference in computing the z component displacement. However, it is important to note the image distortion effect under the presence of the flame and the possible error it can induce, especially when the technique is applied in large-scale flames, as opposed to the laboratory-scale flames investigated here.

4. RESULTS AND DISCUSSION

4.1 Instantaneous and averaged velocity fields

Figure 5 shows sample velocity fields obtained in the experiment. Arrows represent the u (radial) and v (axial) components of the velocity field, in the plane of the laser sheet, while the color contour is used to show the w component, normal to the laser sheet. Red lines in the image show the boundary of the broad thermal zone obtained by the particle seeding density change in the particle image. It is important to note that the broad thermal zone can be different from the flame surface where the heat release rate is the maximum (Paul and Dec, 1994; Watson et al., 1999).

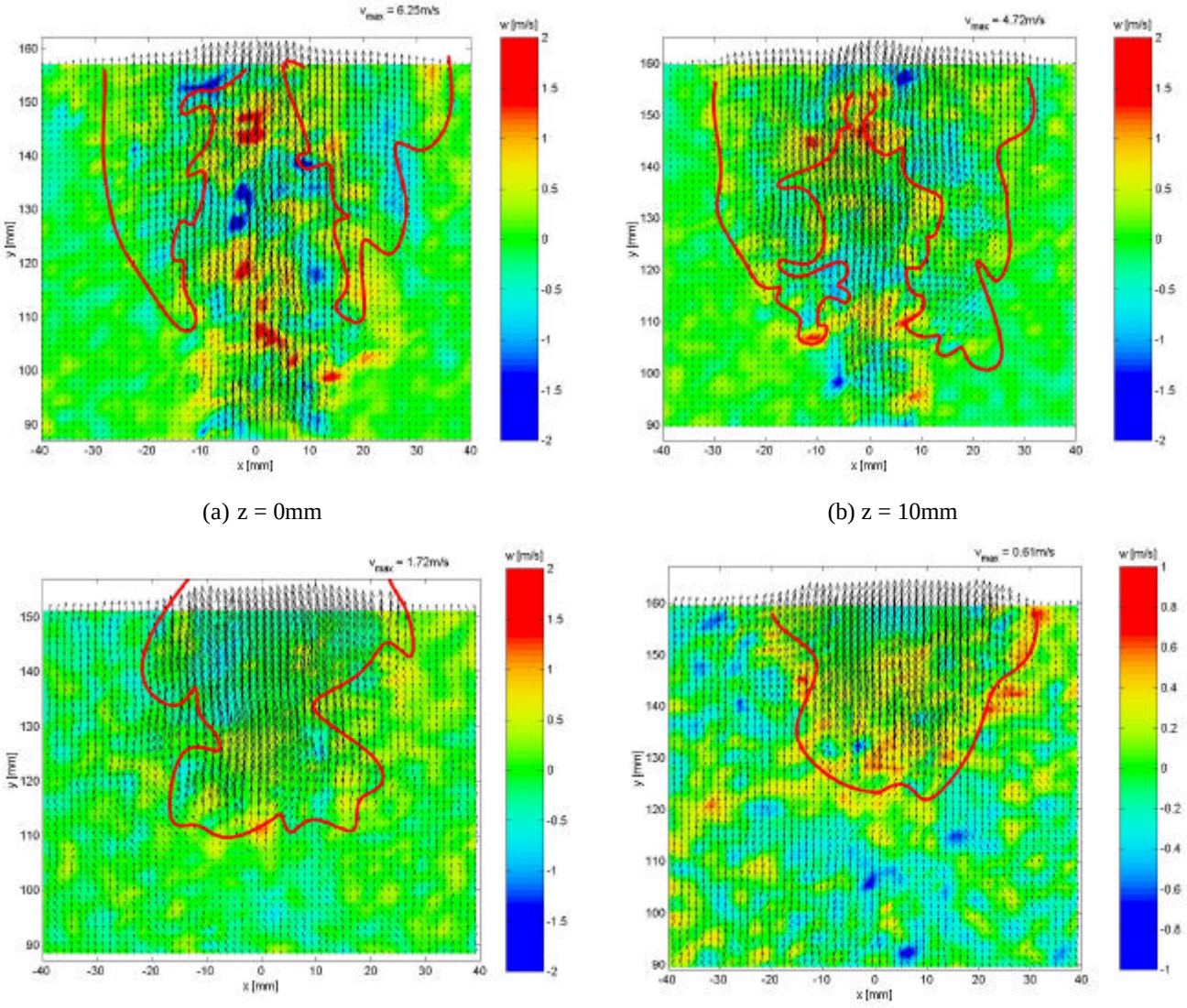

(a) z = 0mm

(b) z = 10mm

(c) z = 20mm

(d) z = 27mm

Fig. 5 Instantaneous velocity fields at the flame base of a lifted flame.

As the image deviates from the center plane (z = 0 plane), two branches of the flame base merge to become a single branch as shown in Fig. 5(c) and (d). In these images, the increase in the flow speed due to the heat release can be clearly observed. However, at the flame base, the flow is observed to diverge and decelerate as observed by previous studies (Muñiz and Mungal, 1997; Schefer and Goix, 1998) for all locations. In addition, the velocity near the centerline shows meandering in both *x* and *z* directions, which seems to imply a spiral structure of the jet which was suggested by Yoda et al. (1994).

Figure 6 shows the average of 120 velocity fields at different *z* planes. The average position of the flame base is obtained by averaging the particle images and using the seeding density change of the averaged image. At the centerline plane, the *w* component of the averaged velocity field does not converge to the expected value of zero. In addition, the *w* component of the coflow stream near the jet in other planes does not converge to zero, contrary to our expectation. It is possible that the measurement method may have induced a systematic error to produce a false value; however, according to the work of Weisgraber and Liepmann (1998), where they obtained the velocity field at fixed axial planes of jets using PIV, the radial component did not show symmetry even after averaging 2000 frames.

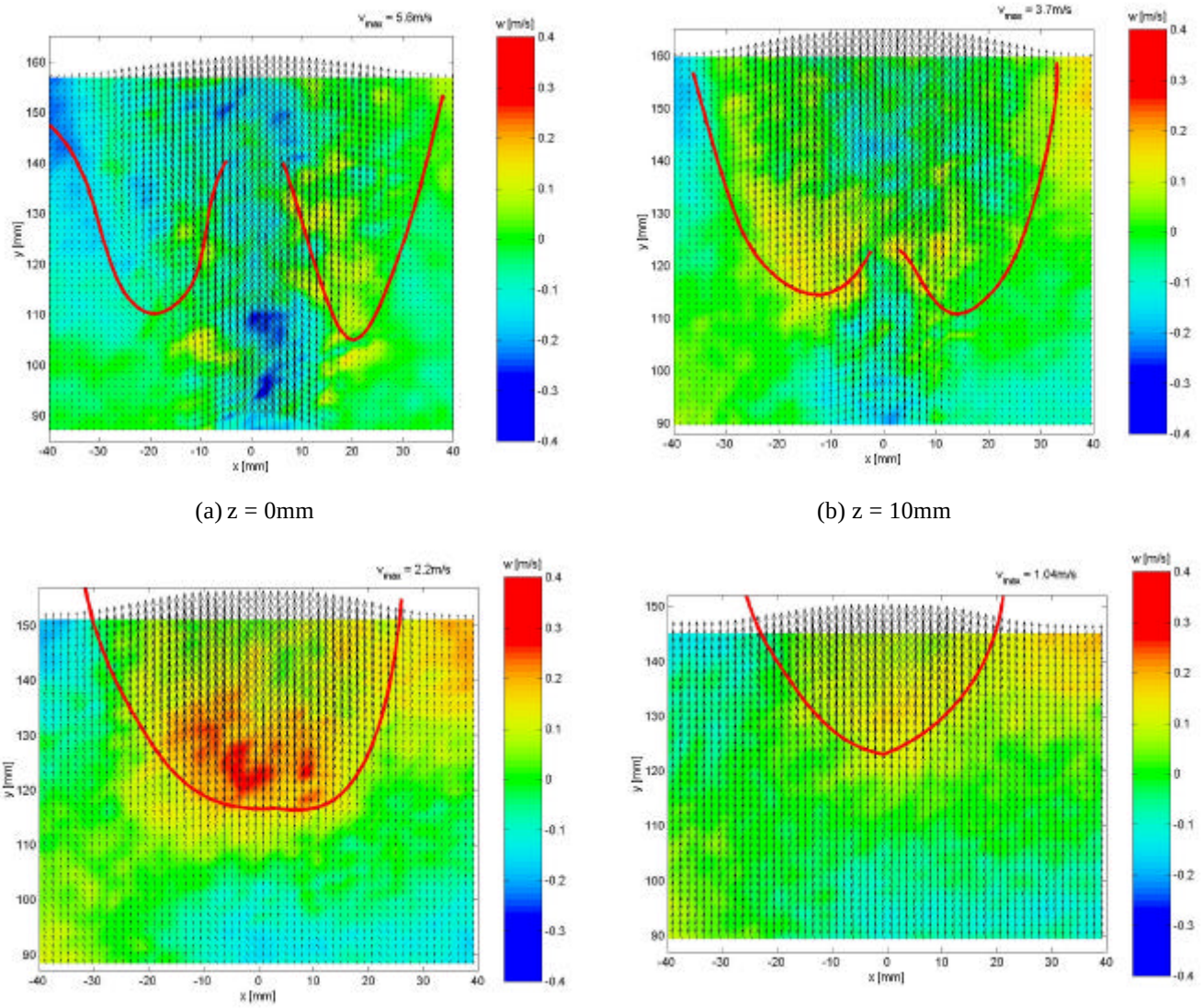

(a) z = 0mm (b) z = 10mm

(c) z = 20mm (d) z = 27mm

Fig. 6 Averaged velocity fields at the flame base of a lifted flame.

They attributed this observation to either the flow structure with a large axial length scale or some mechanism upstream that produces coherent eddies inside the jet. Therefore, it seems plausible that the *w* component does not converge to zero after averaging 120 velocity fields.

Some of the evidence which show the interaction between the flow and the heat release are also observed. At the *z* = 20mm plane in Fig. 6(c), we can observe that the *w* component velocity changes direction as the flow goes through the reacting zone. The dilatation effect caused by the heat release redirects the flow towards the coflow stream.

4.2 Conditional velocity measurement

The velocities at the flame base are measured conditionally. Figure 7 shows the histograms of each velocity component. Since the location of the flame base is determined by the lowest position of the broad thermal zone represented by the particle seeding density, it might not represent the exact position of the flame base. Watson et al. (1999) has shown that the position of the actual heat release measured by CH

planar laser induced fluorescence (PLIF) stays inside the high temperature region measured by OH PLIF. The axial component of the velocity (*v* component) shows a mean speed of $2.39S_L$ with a standard deviation of $1.8S_L$, which corresponds well with previous measurements (Muñiz and Mungal, 1997; Schefer and Goix, 1998; Hasselbrink and Mungal, 1998).

The radial and azimuthal components show similar distribution with the mean near zero. However, the largest value of the *u* and *w* components range up to $2\sim3S_L$, which implies a possible role of these velocity components in the flame stabilization process.

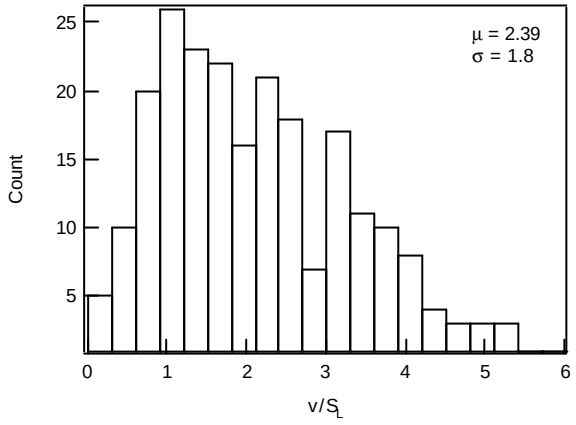

(a) Axial velocity distribution

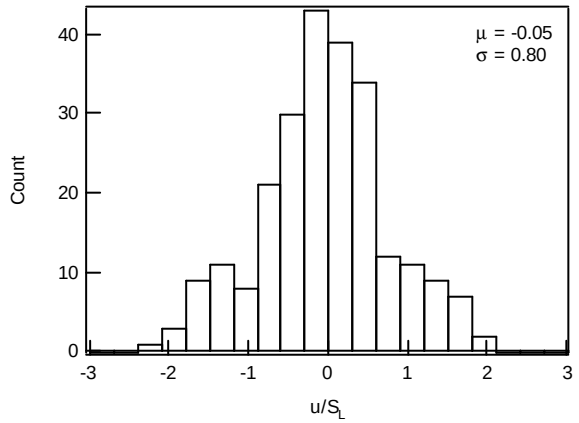

(b) Radial velocity distribution

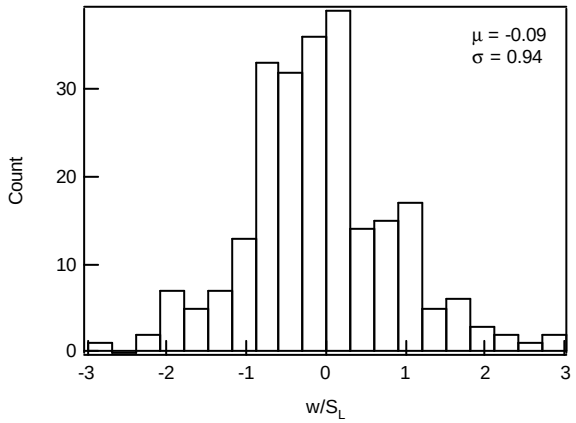

(c) Azimuthal velocity distribution

Fig. 7 Histogram of the conditional velocity measured at the flame base

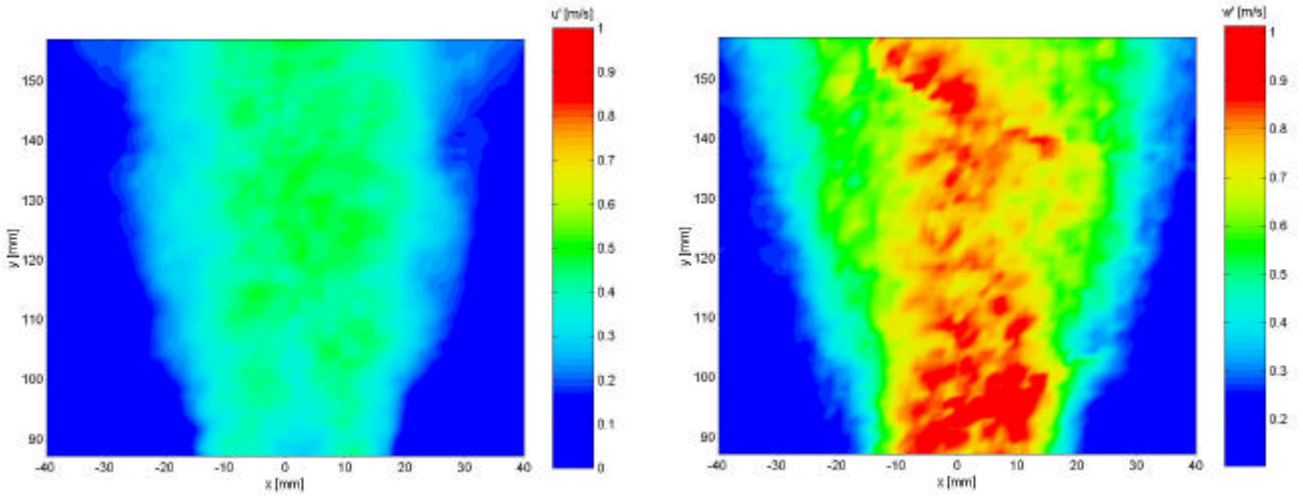

Fig. 8 Turbulent fluctuations at the center plane.

4.3 Turbulent quantities

Since all three component of velocity can be measured, complete information for the turbulent intensities and fluctuations can be obtained in the plane of interest. Since *u* and *w* components are significantly smaller in magnitude than the axial component, *v*, the relative uncertainties involved in these components are larger (Westerweel, 1997). Figure 8 shows the velocity fluctuations of the *u* and *w* components. If we assume that the jet is axisymmetric, the fluctuations at the centerline should be the same in both *x* and *z* directions. However, in this measurement, the fluctuation in the *z* direction is about twice as large as the fluctuation in the *x* direction. This seems to be beyond what we can attribute to the possible problem in the symmetry of the flow. According to the experiment of Lawson and Wu (1997), the RMS displacement error in *z* direction is more than 4 times larger than that in *x* direction at camera angles of 15 degrees, which is close to our experimental setup. Therefore it is possible that the velocity fluctuations in the *z* direction contains significant error induced by the experimental method.

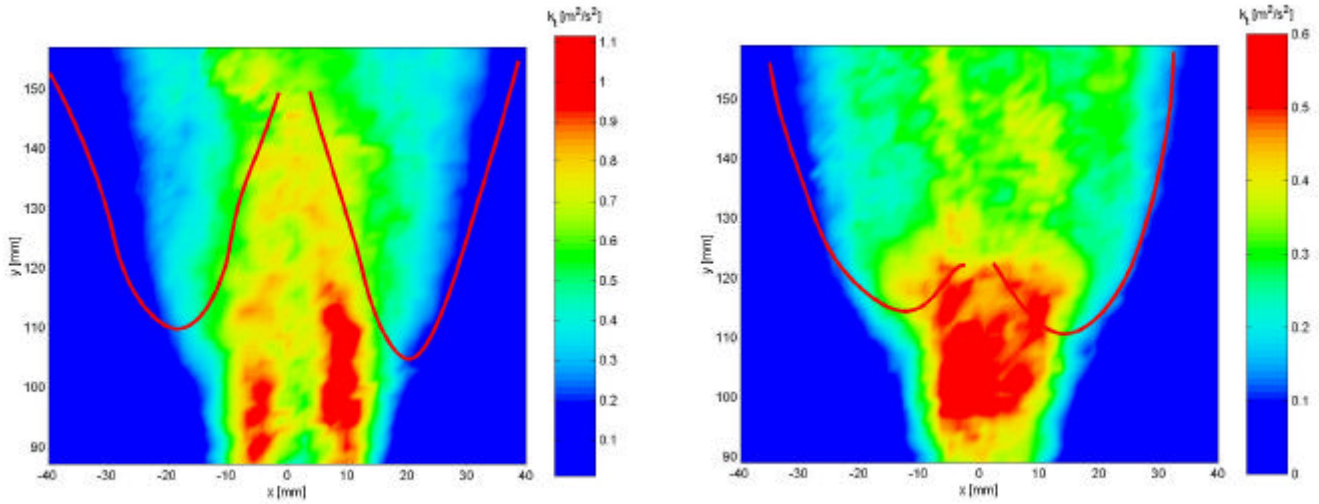

Fig. 9 Turbulent kinetic energy distribution.

Figure 9 shows the turbulent kinetic energy ($1/2(u'^2+v'^2+w'^2)$) distribution along the center (z = 0) plane and z = 10 plane. A reduction in the turbulent kinetic energy can be observed at the broad thermal zone, which is thought to be due to the stabilizing effect of the heat release. In addition, the flame base (marked by the lowest point of the red zone) is observed to reside where the turbulent kinetic energy level becomes relatively low.

5. CONCLUSIONS

Stereoscopic particle image velocimetry (SPIV) is applied at the base of a lifted flame. The influence of the refractive index change due to the heat release on the technique has been investigated using steel ruler images. Main conclusions can be summarized as follows.

1. The refractive index change due to the heat release can distort the image up to 1 pixel for the scale of the flame investigated in this study. If the time delay between two consecutive images is held under the order of msec, the distortion between the images is negligible. Therefore the error in measuring the particle displacement can be minimized by using small time delay.

2. Instantaneous and averaged three component velocity fields at the flame base show complex three-dimensional structures. Their role on the flame stabilization phenomena needs to be investigated in further detail.

3. Conditional velocity measurements performed at the flame base show similar result to previous studies for the axial velocity component. The radial and the azimuthal components show relatively symmetric distributions with the mean value close to zero. However, highest velocities in the radial and azimuthal components are on the order of $2\sim3S_L$, which implies a possible role of these velocity components in flame stabilization.

4. Turbulent kinetic energy distributions show the reduction of the turbulent kinetic energy due to the flame.

5. The flame base is anchored to the location where the turbulent kinetic energy becomes relatively low.

ACKNOWLEDGEMENT

We would like to thank the NSF and the GRI for their support of the work. D. Han acknowledges the support of the Stanford Graduate Fellowship (Mr. and Mrs. Benhamou Fellow).

REFERENCES

BJORKQUIST, D. 1998 Design and calibration of a stereoscopic PIV system. *Proceedings of the Ninth International Symposium on Applications of Laser Techniques to Fluid Mechanics, Lisbon, Portugal*.

BROADWELL, J. E., DAHM, W. J. A. & MUNGAL, M. G. 1984 Blowout of turbulent diffusion flames. *Twentieth Symposium (International) on Combustion, The Combustion Institute, Pittsburgh*, 303-310.

HASSELBRINK, E. F. & MUNGAL, M. G. 1998 Characteristics of the velocity field near the instantaneous base of lifted non-premixed turbulent jet flames. *Twenty-Seventh Symposium (International) on Combustion, The Combustion Institute, Pittsburgh*, 867-873.

LAWSON, N. J. & WU, J. 1997 Three-dimensional particle image velocimetry: experimental error analysis of a digital angular stereoscopic system. *Meas. Sci. Technol.* 8, 1455-1464.

MAUREY, C., CESSOU A. & STEPOWSKI, D. 1998 Simultaneous PIV and OH planar LIF in the stabilization region of a lifted turbulent jet flame. *Proceedings of the Ninth International Symposium on Applications of Laser Techniques to Fluid Mechanics, Lisbon, Portugal*.

MULLER, C. M., BREITBACH, H. & PETERS N. 1994 Partially Premixed Turbulent Flame Propagation in Jet Flames. *Twenty-Fifth Symposium (International) on Combustion, The Combustion Institute, Pittsburgh*, 1099-1106.

MUNIZ, L., MARTINEZ, R. E. & MUNGAL, M. G. 1996 Application of PIV to Turbulent Reacting Flows. *Proceedings of the Eighth International Symposium on Applications of Laser Techniques to Fluid Mechanics, Lisbon, Portugal*, 411-424.

MUNIZ, L. & MUNGAL, M. G. 1997 Instantaneous Flame-Stabilization Velocities in Lifted-Jet Diffusion Flames. *Combust. Flame* 111, 16-31.

PAUL, P. H. & DEC, J. E. 1994 Imaging of reaction zones in hydrocarbon-air flames by use of planar laser induced fluorescence of CH. *Optics Letters* 19, 998-1000.

PETERS, N. & WILLIAMS, F. A. 1983 Liftoff characteristics of turbulent jet diffusion flames, *AIAA Jr.* 21, 423-429.

PITTS, W. M. 1988 Assessment of theories for the behavior and blowout of lifted turbulent jet diffusion flames. *Twenty-Second Symposium (International) on Combustion, The Combustion Institute, Pittsburgh*, 809-816.

SCHEFER R. W. & GOIX P. J. 1998 Mechanism of flame stabilization in turbulent, lifted-jet flames. *Combust. Flame* 112, 559-574.

SOLOFF S. M., ADRIAN, R. J. & LIU Z-C. 1997 Distortion compensation for generalized stereoscopic particle image velocimetry. *Meas. Sci. Technol.* 8, 1441-1454.

VANQUICKENBORNE, I. & VAN TIGGELEN, A. 1966 The stabilization mechanism of lifted diffusion flames, *Combust. Flame* 10, 59-69.

WATSON, K. A., LYONS K. M., DONBAR, J. M. & CARTER, C. D. 1999 Observation on the leading edge in lifted flame stabilization, *Combust. Flame* 117, 257-271.

WEISGRABER, T. H. & LIEPMANN, D. 1998 Turbulent structure during transition to self-similarity in a round jet. *Experiments in Fluids* 24, 210-224.

WESTERWEEL, J. 1997 Fundamentals of digital particle image velocimetry. *Meas. Sci. Technol.* 8, 1379-1392.

YODA, M., HESSELINK, L., & MUNGAL, M. G. 1994 Instantaneous three-dimensional concentration measurements in the self-similar region of a round high-Schmidt-number jet. *J. Fluid Mech.* 279, 313-350.